Ferromagnetic resonance in a microtube

V. A. Fel'k[1,a)] (ID) and S. V. Komogortsev[2,b)] (ID)

AFFILIATIONS

[1]Reshetnev Siberian State University of Science and Technology, Krasnoyarsk 660049, Russia
[2]Kirensky Institute of Physics, Federal Research Center Krasnoyarsk Science Center, Siberian Branch, Russian Academy of Sciences, Krasnoyarsk 660036, Russia

[a)]**Author to whom correspondence should be addressed:** vlaf80@mail.ru
[b)]**Electronic mail:** komogor@iph.krasn.ru

ABSTRACT

Ferromagnetic resonance fields in a microtube with various ratios of the inner and outer diameter of the tube β were studied using micromagnetic simulation. For $\beta < 0.15$, the resonance field agrees with the prediction of the Kittel equation for an infinite ferromagnetic cylinder for both parallel and perpendicular orientation of the applied field to its axis. For $\beta > 0.15$, the resonance field increases from the resonance field of the infinite cylinder and approaches the level of a film magnetized along the plane. This behavior only qualitatively agrees with the prediction made using the calculated demagnetizing factor in the ferromagnetic tube. For $\beta > 0.15$ and the applied transverse field, a number of resonance peaks were observed for the microtube with the outer diameter of 500 nm, but for nanotubes with the diameters of 50 and 100 nm, a single peak was observed.

Published under an exclusive license by AIP Publishing. https://doi.org/10.1063/5.0045548

I. INTRODUCTION

Ferromagnetic micro- and nanotubes are of interest as a functional elements for various advanced applications such as biomedicine, catalysis, magnetic force microscopy tips, microwave applications and magnonics,[1–6] and racetrack memory.[7] The understanding of relationship between the static and dynamic magnetic behavior,[8–15] including magnetic resonance[16–22] and the atomic and magnetic structure of the material,[23–27] is necessary for designing its properties. The magnetization dynamics in a ferromagnetic element is determined by its material parameters, size, and shape. The latter makes ferromagnetic resonance (FMR) a sensitive experimental tool for characterizing micro- and nanoelements, in particular, micro- and nanotubes. One of the difficulties of theoretical FMR calculations in the tube is due to the fact that the demagnetizing tensor is nonuniform for this shape. The elements of this tensor (demagnetizing factors) for specific shapes allow one to calculate the demagnetizing field in samples with the non-ellipsoidal shape. In practice, the nonuniform demagnetizing field is replaced by an average one according to the sample.[28] This idea was used for analytical calculations of the demagnetizing factor of the tube.[29–31] The calculated factor was applied for the interpretation of some experiments on magnetic nanotubes.[32,33] In our opinion, the applicability of the average demagnetizing factor for the tube

needs to be verified. The field at which the maximum on the FMR curves is observed is determined by the internal magnetic field. Therefore, a correlation between the internal field and the tube parameters can be established using the FMR study. In particular, in this way, the analytical results for the demagnetizing field of the tube can be tested. The results of micromagnetic calculation of the resonance fields H_r in the tubes with various ratios of the inner diameter to the outer one $\beta = D_{in}/D_{out}$ are presented in the paper. The results are compared with the dependences calculated using the previously derived analytical expression for the tube demagnetizing factor. The behavior of $H_r(\beta)$ for two cases, the field applied parallel and perpendicular to the tube axis, is discussed.

II. MODEL AND NUMERICAL EXPERIMENT

The magnetization **M** within the micromagnetic approximation is presented by a continuous vector field.[34] We describe the dynamics of a ferromagnetic medium by the classical Landau–Lifshitz–Gilbert (LLG) equation

$$\frac{d\mathbf{M}}{dt} = -\gamma(\mathbf{M} \times \mathbf{H}_{eff}) - \frac{\gamma\sigma}{M_s}\mathbf{M} \times (\mathbf{M} \times \mathbf{H}_{eff}), \quad (1)$$

where **M** is the magnetization, γ is the gyromagnetic ratio [$\gamma = 2.211 \times 10^5$ m/(A s)], σ is the damping constant, M_s is the

saturation magnetization, and $\mathbf{H}_{eff}$ is the effective local magnetic field, which is determined by the expression

$$\mu_0 \mathbf{H}_{eff} = -\frac{\partial \mathscr{H}}{\partial \mathbf{M}} + \frac{\partial}{\partial \mathbf{x}} \frac{\partial \mathscr{H}}{\partial (\partial \mathbf{M}/\partial \mathbf{x})}. \quad (2)$$

We choose the energy density $\mathscr{H}$ in the form

$$\mathscr{H} = \mu_0 \left(\frac{1}{2}\alpha \left(\frac{\partial \mathbf{M}}{\partial \mathbf{x}} \right)^2 - \mathbf{MH} - \frac{1}{2}\mathbf{MH}_m \right), \quad (3)$$

where $\alpha = 2A/(\mu_0 M^2)$ is the exchange parameter (A is the exchange stiffness), $\mathbf{H}$ is the external magnetic field, $\mathbf{H}_m$ is the magneto-dipole field, and $\mathbf{x} = (x, y, z)$. In our simulations, we choose the value of γ that assumes the g-factor to equal 2. Note that the interpretation of the calculations in connection with the experiment may require a correction for the magnetization and gyromagnetic ratio relevant for the tube material.[35]

Integration of the LLG equation was performed using the OOMMF[36,37] micromagnetic code. The outer diameter of the tube D_{out} was chosen to be 500 nm. The periodic boundary conditions (PBC) were applied along the tube axis for the dipole–dipole and exchange interactions. Such conditions assume that the tube of infinite length is simulated (the length of the periodically repeated fragment along the z axis was $L = 15$ nm). According to the purposes, tubes of different inner diameter D_{in} were simulated, and all further results are presented, depending on the parameter $\beta = D_{in}/D_{out}$.

In the micromagnetic simulation, the cell size should not exceed the exchange length $\lambda_{ex} = \sqrt{2A/(\mu_0 M_s^2)}$ ($\lambda_{ex} \approx 13$ nm for our parameters).[38,39] We used a cubic cell with the size of $cs = 5$ nm. For such a cell, the reliable simulation results can be expected despite the irregularities of the outer and inner boundaries of the tube due to the cell structure of the tube.[40–42] The following tests prove the appropriateness of this choice. The following material parameters were used: the saturation magnetization $M_s = 3 \times 10^5$ A/m and uniform exchange stiffness $A = 10^{-11}$ J/m. The dipole energy was calculated based on the assumption that the magnetization is constant in each cell.[28,43,44] The damping constant was $\sigma = 0.05$, which is close to the value for Ni.[45–47] The magnetization value of 3×10^5 A/m is chosen because in this case, the resonance fields of the tube would be positive both for the parallel and perpendicular orientation of the field to the tube axis. This value is close to the magnetization for NiP coatings obtained by electrolytic and electroless deposition[48] often used for preparing micro- and nanotubes in porous templates.[49,50]

The major hysteresis loops were calculated using the initial state with the uniform magnetization, where the changes in the micromagnetic configurations and the magnetization curve are reversible. The fields were changed in the following sequence $H_{max} \rightarrow -H_{max} \rightarrow H_{max}$. To avoid the occurrence of artifact metastable states, we used small deviations from the ordered state.

There are various approaches to the FMR simulation:[51,52] the time evolution method,[53] the ringdown method,[54] and the eigenvalue method.[55–58] For the simulation, we used the first approach. The amplitude of the magnetization oscillations was calculated depending on the applied constant (dc) field. This provides
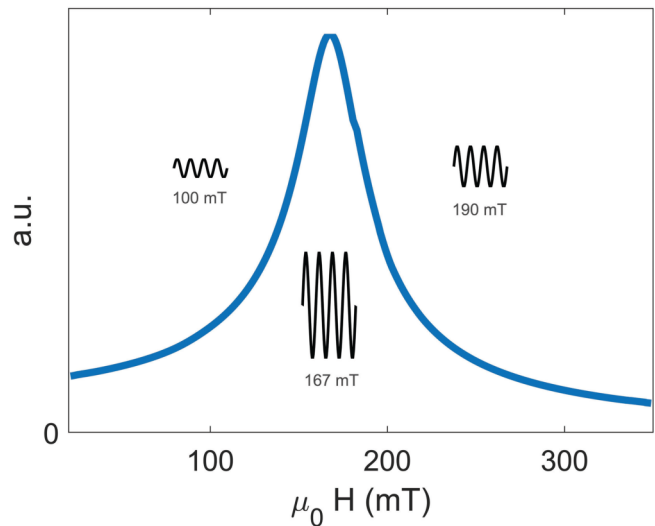

FIG. 1. The calculated resonance line at an example of the tube with $\beta = 0.67$ and dc-field along the tube axis.

information as is done in many spectrometric techniques (for example, Refs. 59–62). In this approach, a sinusoidal field of the microwave range (ac) of a fixed frequency and a small amplitude is applied to the system $H_{ac} = H_{ac,0}\sin(\omega t)$. The dc-field is applied perpendicular to the ac-field (at a fixed frequency of the ac-component), and the magnetization precession is calculated. The final dependence of the magnetization precession amplitude vs the applied field is the FMR curve (Fig. 1) (see Sec. 1 in the supplementary material). Further results are calculated for two directions of the dc-field: parallel and perpendicular to the tube axis. The frequency of the ac-field $f = \omega/(2\pi) = 9.37$ GHz is used, which is close to the one usually applied in experimental X-band equipment.[59–62] The value of the ac-field $\mu_0 H_{ac,0} = 0.5$ mT (much lower than the dc-field) is used to avoid nonlinear oscillatory dynamics. As an example in Fig. 1, the FMR curve at a fixed β and with the parallel orientation of the dc-field to the tube axis is shown. The time step may change during the calculations, but it is limited by 10^{-12} s.

The correct choice of the cell size is of importance for simulating the magnetic dynamics.[63,64] The effect of the cell size on FMR was estimated by comparing the FMR results for different cell sizes. The resonance curves for three cell sizes: 5, 10, and 20 nm show that the cell of 5 nm can be considered adequate for good accuracy of results (see Sec. 2 in the supplementary material).

III. RESULTS OF THE NUMERICAL EXPERIMENT AND DISCUSSION

A. Magnetization curves

FMR was calculated in the fields corresponding to the magnetic saturation (Fig. 2). The magnetization shows a linear response [Fig. 2(b)] in small fields for the perpendicular orientation of the
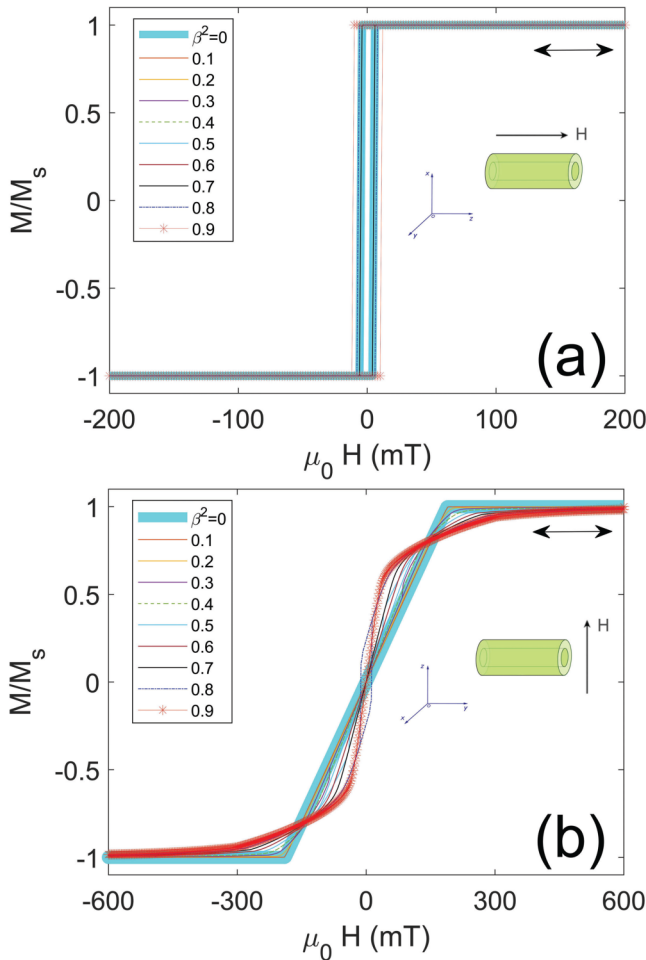
FIG. 2. Hysteresis loops in the tube for different β with the dc-field along (a) and transverse to the tube axis (b). The two-sided arrows show the field range where FMR is observed.

FIG. 3. Demagnetizing field in the tube with various wall thicknesses. The solid curve corresponds to Eq. (4).

dc-field to the tube axis. At $\beta = 0$ (solid cylinder), the magnetization increases linearly with the growth of the field to $H_d = \frac{1}{2}M_s$, which is equal to the demagnetizing field[65] [Fig. 2(b)]. The magnetization curves of the tube ($\beta > 0$) show a sharper linear increase than it is for a solid cylinder as the tube wall becomes thinner. The fields limiting the linear response for the tubes are smaller than H_d, and above these fields, the magnetization behaves non-linearly. The description of the linear response as $M = H/H_d$ allows us to estimate the magnitude of the demagnetizing field H_d for the tubes with various wall thicknesses. The behavior $H_d(\beta)$ is very well fitted (Fig. 3) by the following equation:

$$H_d = \frac{1}{2}M_s(1 - \beta^2). \tag{4}$$

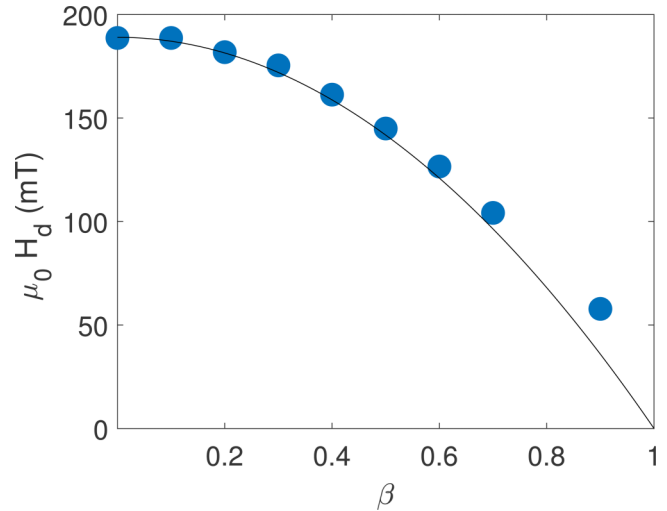In the saturation regime, the magnetization of the tube is almost uniform. In this case, it seems that a constant

demagnetizing factor can be used. For the ferromagnetic tube in a number of studies,[29–31] the following analytical expression for the demagnetizing factor was derived:

$$N_y = \frac{D_{out}}{L(1 - \beta^2)}\int_0^\infty \frac{dq}{q^2}(J_1(q) - \beta J_1(\beta q))^2(1 - e^{-(2q/L)D_{out}}). \tag{5}$$

Here, $J_1(z)$ is the first-order and first-kind Bessel function and L is the tube length. According to this expression, the main contribution to the demagnetizing factor of a very long tube is the ratio of the outer diameter of the tube to its length, while the wall thickness makes only a slight correction. In the limit $D/L \rightarrow 0$ (the infinite tube limit that is realized in our case by PBC along the tube axis), we have $N_y \rightarrow 0$. Therefore, $N_x = N_z = (1 - N_y)/2 \rightarrow 1/2$. In this case, one can expect that the tube will behave identically to the infinite cylinder for all β.

The data in Fig. 3 described with Eq. (4) are in excellent agreement with the analytical result of Ref. 66. The demagnetizing factor determined from the magnetization curve in Fig. 2(b) according to Ref. 66 is the so-called magnetometric demagnetizing factor. Since the magnetocrystalline anisotropy is not taken into account (the magnetic anisotropy constant is zero), the permeability of the tube medium tends to infinity (extremely soft magnetic material). The empirically found equation (4) completely repeats the result of Ref. 66, $N_z = \frac{1}{2}(1 - \beta^2)$, taking into account the coordinate system shown in the inset of Fig. 2(b).

B. Constant field along the tube axis

The intensity and width of the FMR peak in the tube with the field applied along its axis remain constant, but the resonance field increases with the increase in β (Fig. 4). The resonance associated with a uniform mode of the magnetization oscillations is to be
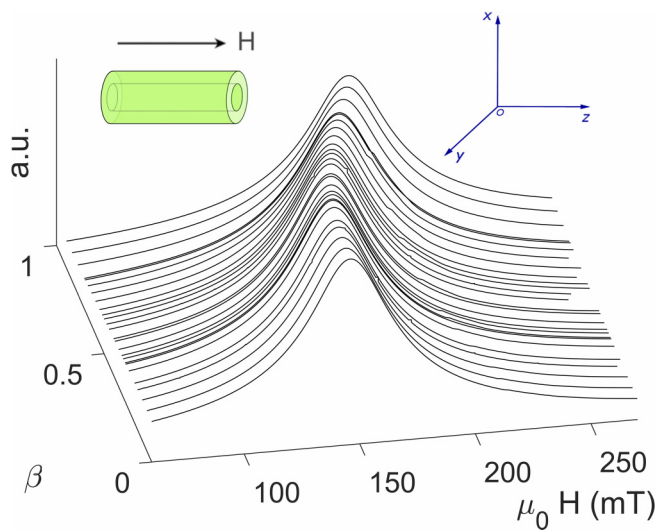
FIG. 4. Ferromagnetic resonance in the tube magnetized along its axis for various β.

expected near the field predicted by the Kittel equation,[67,68]

$$\omega^2 = \gamma^2[H + (N_x - N_z)M][H + (N_y - N_z)M], \quad (6)$$

where N_x, N_y, and N_z are the demagnetization factors along the x, y, and z directions, which satisfy the relation $N_x + N_y + N_z = 1$.

At $\beta < 0.15$, the resonance field H_r (see Fig. 5) is close to the prediction of the Kittel equation (6) for the infinitely long cylinder
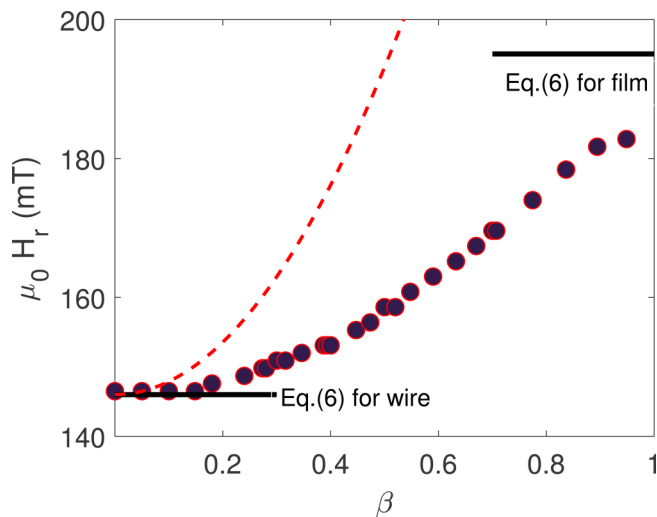

FIG. 5. Resonant field H_r vs β for the tube magnetized along its axis ($\bullet$). The dotted line corresponds to Eq. (7). The solid lines correspond to the predictions of Eq. (6) for the film and for the wire.

($N_x = 1/2$, $N_y = 1/2$, $N_z = 0$, $\mu_0 H_r = 146$ mT). The coincidence of the solution of Eq. (6) and the results of the numerical experiment in this "trivial case" ($\beta = 0$) imply the correctness of the numerical procedures used (including PBC) and reliability of the obtained data on the magnetization dynamics. One will expect that for small β, the dynamics of the tube magnetization is represented by the uniform mode as in the infinite cylinder. The observations of the magnetic dynamics patterns (Sec. 3 in the supplementary material) show that for the field along the tube axis, the uniform precession dynamics is realized for all the beta. However, at $\beta > 0.15$, the resonant field differs from the field of the infinite cylinder. For $\beta > 0.15$, the resonance field increases (Fig. 5), and for β close to unity, it approaches the resonance field of an infinite film magnetized in the tangent direction (for $N_x = 0$, $N_y = 0$, $N_z = 1$, $\mu_0 H_r = 195.5$ mT). It is clear to look at the tube walls for a film twisted around the tube axis. When the outer diameter tends to ∞ and $\beta \to 1$, the tube becomes equivalent to the film. In Fig. 5, when β approaches 1, H_r tends to a value slightly smaller than 195.5 mT (film resonance), which is due to the dipole–dipole interaction of magnetization of the opposite tube walls because of the finite outer diameter (500 nm). As shown above, according to Refs. 25, 30, and 31, the infinite tube would behave identically to the infinite cylinder for all β. Particularly, this means that H_r would not depend on β and would be equal to the resonance field of the infinite cylinder for any β. However, the numerical experiment demonstrates other behavior. The transition between the limits of the "infinite cylinder" and the "thin film" for the tubes with various wall thicknesses is observed. Such behavior apparently would be universal for tubes with different material parameters and sizes.

To analytically describe the transition between these two limits (cylinder and film), the empirically established equation (4) for the demagnetizing field and Eq. (6) were used. In this case, the resonance field is written as

$$H_r = \frac{\omega}{\gamma} - \frac{1}{2}M_s(1 - \beta^2). \quad (7)$$

The dotted curve in Fig. 5 corresponds to this equation. The predictions of Eq. (7) correspond qualitatively to the calculated resonance fields, but the quantitative agreement with the numerical experiment is obtained only in the vicinity of $\beta \approx 0$, i.e., when the diameter of the inner cavity of the tube is small.

C. Constant field perpendicular to the tube axis

In the field applied across the tube axis, a single peak is observed at small β, and then, it splits into several peaks (Fig. 6) with the increase in β. Additionally, the sequences of peaks (branches) are visually highlighted. The position, intensity, and width of the FMR lines, depending on beta, change in a different manner. The resonance fields of some peaks increase with β, and some of them decrease.

The FMR intensities within some branches decrease with the increasing β and disappear at sufficiently large β, while some branches appear at certain values of β as a result of splitting (bifurcations) the existing peaks and they are retained up to $\beta = 1$.
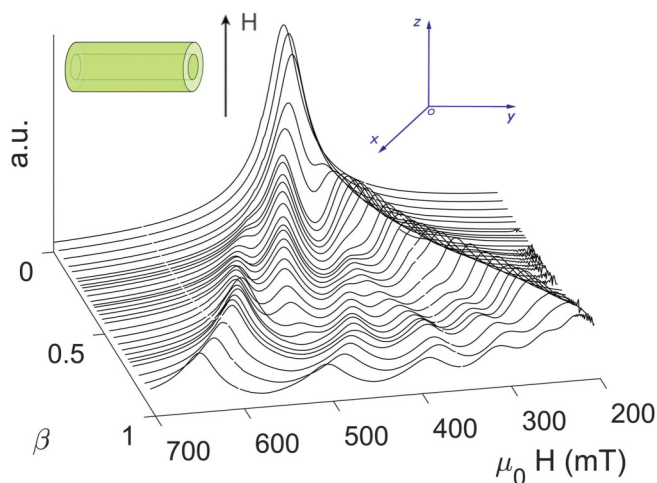
FIG. 6. Ferromagnetic resonance in the transversely magnetized tube for various values of β.

Bifurcations are observed at $\beta = 0.15, 0.30, 0.39, 0.50,$ and 0.67. The number of peaks in Fig. 7 varies from one to six. The six peaks are observed only at $\beta = 0.67$. With an increase in β above 0.67, one observes five peaks. The resonance field at $\beta < 0.15$ corresponds to the solution of Eq. (6) for the infinitely long cylinder (Fig. 7). For such a small β in the tube, one may expect that there is a uniform mode of the magnetization dynamics. The observations of the magnetization dynamics show that this is not the case (Sec. 3 in the supplementary material). The uniform precession occurs only for $\beta = 0$ (solid cylinder). In the samples with any
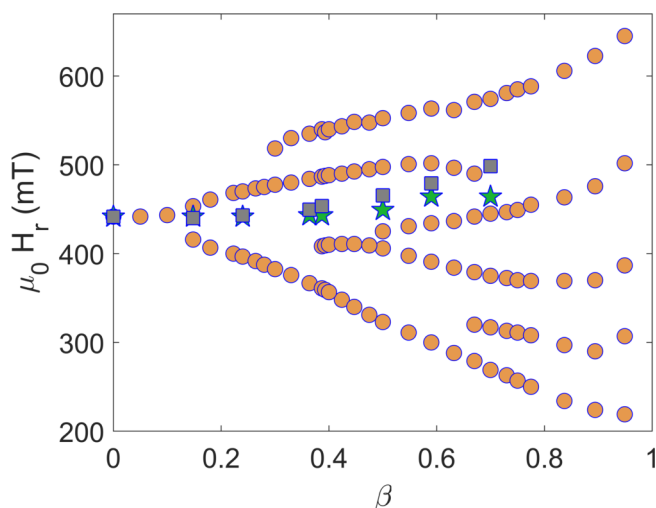
other $\beta \neq 0$, including the cases of the tubes at $0 < \beta < 0.15$, where a single resonance peak is obtained located in the field close to the resonance field of the infinite cylinder, nonuniform modes are observed (Sec. 3 in the supplementary material).

The tube thickness limits the wavelength of the non-uniform magnetization modes. The range of the tube wall thicknesses used in our calculations corresponds to the range of the wave numbers $k = 4 \times 10^4 - 4 \times 10^5 \, \text{cm}^{-1}$. At such wave numbers, the dipole-exchange modes in the magnetic dynamics are expected.[69–71]

To explain the multiplicity of peaks in the transverse field for the tube with an outer diameter of 500 nm, let us use the argument already discussed in Sec. III B that one can look at the walls of the tube as if it were a film twisted around the tube axis. In the transverse field, the parts of the film constituting the tube wall perpendicular to the field should provide resonance in a high field ($\mu_0 H_r = 712 \, \text{mT}$), while the side parts of the walls would result in resonances like in the film magnetized along the field ($\mu_0 H_r = 196 \, \text{mT}$). Note that all the observed peaks lie between these two values. In addition, the lowest-field and highest-field peaks have the largest amplitudes, indicating that they are dominant. It can be assumed that the tube with the diameter of 500 nm is too large, and it leads to an inhomogeneity of the internal field, which, in turn, leads to the appearance of a number of resonant peaks. In order to test this idea, taking into account the noticeable interest to this field of study with the use of nanotubes from 40 to 100 nm in diameter, we carried out additional calculations of FMR in the tubes with the diameter of 50 and 100 nm.

One would expect that the number of the FMR peaks would decrease due to the exchange interactions between the neighboring regions with different internal fields. Indeed, in the tubes with the outer diameter of 50 and 100 nm, a single absorption peak is observed (Fig. 8). According to Fig. 7, the resonance field of this
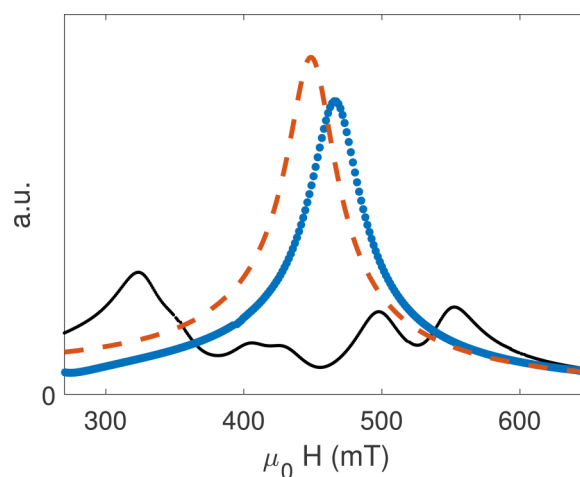

FIG. 7. Resonance fields in the transverse orientation of the dc-field. ● ($D_{out} = 500 \, \text{nm}$), ■ ($D_{out} = 100 \, \text{nm}$), and ★ ($D_{out} = 50 \, \text{nm}$).

FIG. 8. Resonance fields in the transverse orientation of the dc-field for three values of the outer diameter of the tube ($\beta = 0.5$): solid line ($D_{out} = 500 \, \text{nm}$), snowball ($D_{out} = 100 \, \text{nm}$), and dotted line ($D_{out} = 50 \, \text{nm}$).

peak in the tubes with the outer diameter of 50 and 100 nm slightly increases with the increasing β. It is worth noting that the calculated data were obtained for a single tube. Since nano- and microtubes are mainly obtained and investigated inside alumina templates or polycarbonate membranes, it should be noted that in this case, the interaction between the tubes can affect the position of the resonance peaks.[72,73] The reported results for a single tube would be useful for describing resonance in samples with a low fill factor.

IV. CONCLUSION

The dependences of the ferromagnetic resonance fields on the ratio of the inner diameter of the tube to the outer diameter β were studied for a ferromagnetic microtube with the magnetization of $M_s = 3 \times 10^5$ A/m and an external diameter of 500 nm and nanotubes 50 and 100 nm in diameter. The periodic boundary conditions along the tube axis were used to simulate a very long (infinite) tube. The resonance field was found to agree with the prediction of the Kittel equation for the infinite cylinder for the tube with $\beta < 0.15$. The resonance field in the case of the field along the tube axis increases with β, tending to a certain value at $\beta \to 1$ close to the field of the tube with very thin walls. The empirical correlation of the magnetometric demagnetizing factor established from the magnetization curves is in agreement with the latest analytical results of Prat-Camps *et al.* The numerical experiment on the resonance field behavior demonstrates that at $\beta > 0.15$, the behavior is slightly different from what could be expected from the observed magnetometric demagnetizing factor behavior vs β. The transition between the limits of the "infinite cylinder" and the "thin film" for the tubes with various wall thicknesses would apparently be universal for tubes with different material parameters and sizes. Several resonance peaks are observed for the field transverse to the tube axis and at $\beta > 0.15$ in the microtube of 500 nm in diameter, while a single peak was observed in the nanotubes with the diameter of 50 and 100 nm.

SUPPLEMENTARY MATERIAL

See the supplementary material that includes clarification of the following issues: 1. Algorithm for extracting the amplitude of magnetization. 2. The effect of the cell size to the FMR and hysteresis curves. 3. Visualization of magnetic dynamics.

DATA AVAILABILITY

The data that support the findings of this study are openly available in Materials Cloud at https://doi.org/10.24435/materialscloud:he-d6, Ref. 74.

REFERENCES

[1]M. Stano and O. Fruchart, *Handbook of Magnetic Materials* (North-Holland/American Elsevier, Amsterdam, 2018), p. 155.

[2]*Handbook of Nanophysics*, edited by K. D. Sattler (CRC Press Taylor & Francis Group, Boca Raton, FL, 2011), Vol. 4.

[3]B. X.-F. Han, S. Shamaila, R. Sharif, J.-Y. Chen, H.-R. Liu, and D.-P. Liu, Adv. Mater. **21**, 4619 (2009).

[4]L. Xiao-Li, Y. Yong, W. Jian-Peng, Z. Yi-Fan, F. Hai-Ming, and D. Jun, Chin. Phys. B **24**, 127505 (2015).

[5]S. Xue, C. Cao, D. Wang, and H. Zhu, Nanotechnology **16**, 1495 (2005).

[6]Q. Fu, Y. Li, L. Chen, F. Ma, H. Li, Y. Xu, B. Liu, R. Liu, and Y. Du, Chin. Phys. Lett. **37**, 087503 (2020).

[7]B. Zingsem, M. Farle, T. Feggeler, and I. Iglesias, U.S. patent 10,614,902 (7 April 2020).

[8]R. Sharif, S. Shamaila, M. Ma, L. D. Yao, R. C. Yu, X. F. Han, and M. K. ur Rahman, Appl. Phys. Lett. **92**, 032505 (2008).

[9]A. P. Chen, J. Gonzalez, and K. Guslienko, Materials **101**, 11 (2018).

[10]Y. G. Yoo, M. Klaui, C. A. F. Vaz, L. J. Heyderman, and J. A. C. Bland, Appl. Phys. Lett. **82**, 2470 (2003).

[11]M. P. Proenca, C. T. Sousa, J. Escrig, J. Ventura, M. Vazquez, and J. P. Araujo, J. Appl. Phys. **113**, 093907 (2013).

[12]D. G. Chaves-O'Flynn, A. D. Kent, and D. L. Stein, Phys. Rev. B **79**, 184421 (2009).

[13]D. Richardson and F. M. F. Rhen, Phys. Procedia **75**, 1158 (2015).

[14]D. Richardson and F. M. F. Rhen, IEEE Trans. Magn. **51**, 2301504 (2015).

[15]J. A. Fernandez-Roldan, D. Chrischon, L. S. Dorneles, O. Chubykalo-Fesenko, M. Vazquez, and C. Bran, Nanomaterials **8**, 692 (2018).

[16]Z. K. Wang *et al.*, Phys. Rev. Lett. **94**, 137208 (2005).

[17]J. Podbielski, F. Giesen, and D. Grundler, Phys. Rev. Lett. **96**, 167207 (2006).

[18]G. Gubbiotti, M. Madami, S. Tacchi, G. Carlotti, H. Tanigawa, T. Ono, L. Giovannini, F. Montoncello, and F. Nizzoli, Phys. Rev. Lett. **97**, 247203 (2006).

[19]A. L. González, P. Landeros, and A. S. Núñez, J. Magn. Magn. Mater. **322**, 530 (2010).

[20]G. Chai, X. Wang, M. S. Si, and D. Xue, Phys. Lett. A **377**, 1491 (2013).

[21]L. A. Chekanova, E. A. Denisova, R. N. Yaroslavtsev, S. V. Komogortsev, D. A. Velikanov, A. M. Zhizhaev, and R. S. Iskhakov, Solid State Phenom. **233**, 64 (2015).

[22]B. Nam, J. Kim, and K. K. Hyeon, J. Appl. Phys. **111**, 07E347 (2012).

[23]P. Landeros, J. Escrig, D. Altbir, M. Bahiana, and J. d'Albuquerque e Castro, J. Appl. Phys. **100**, 044311 (2006).

[24]V. P. Kravchuk, D. D. Sheka, and Y. B. Gaididei, J. Magn. Magn. Mater. **310**, 116 (2007).

[25]J. Escrig, P. Landeros, D. Altbir, and E. E. Vogel, J. Magn. Magn. Mater. **310**, 2448 (2007).

[26]C. Sun and V. L. Pokrovsky, J. Magn. Magn. Mater. **355**, 121 (2014).

[27]A. Riverosa, N. V. Silva, P. Landeros, D. Altbir, E. E. Vogel, and J. Escrig, J. Magn. Magn. Mater. **401**, 848 (2016).

[28]A. Aharoni, J. Appl. Phys. **83**, 3432 (1998).

[29]J. Escrig, P. Landeros, D. Altbir, E. E. Vogel, and P. Vargas, J. Magn. Magn. Mater. **308**, 233 (2007).

[30]J. Escrig, M. Daub, P. Landeros, K. Nielsch, and D. Altbir, Nanotechnology **18**, 445706 (2007).

[31]M. Beleggia, D. Vokoun, and M. D. Graef, J. Magn. Magn. Mater. **321**, 1306 (2009).

[32]R. Lavin, J. C. Denardin, J. Escrig, D. Altbir, A. Cortes, and H. Gomez, J. Appl. Phys. **106**, 103903 (2009).

[33]M. P. Proenca, C. T. Sousa, J. Ventura, J. P. Araujo, J. Escrig, and M. Vazquez, Spin **2**, 1250014 (2012).

[34]W. F. Brown, *Micromagnetics* (Interscience, New York, 1963).

[35]C. T. Sousa *et al.*, J. Nanosci. Nanotechnol. **12**, 7486 (2012).

[36]M. Donahue and D. Porter, *Object Oriented Micromagnetic Framework (OOMMF)* [The National Institute of Standards and Technology (NIST), Gaithersburg, 2006].

[37]M. J. Donahue and D. G. Porter, see https://nanohub.org/resources/oommf for "OOMMF: Object Oriented MicroMagnetic Framework" (2016).

[38]S. V. Komogortsev, V. A. Fel'k, R. S. Iskhakov, and G. V. Shadrina, J. Exp. Theor. Phys. **125**, 323 (2017).

[39]G. S. Abo, Y.-K. Hong, J. Park, J. Lee, W. Lee, and B.-C. Choi, IEEE Trans. Magn. **49**, 4937 (2013).

[40]S. V. Komogortsev, V. A. Fel'k, and O. A. Li, J. Magn. Magn. Mater. **473**, 410 (2019).

[41]C. J. Garcia-Cervera, Z. Gimbutas, and E. Weinan, J. Comput. Phys. **184**, 37 (2003).

[42]M. J. Donahue and R. D. McMichael, IEEE Trans. Magn. **43**, 2878 (2007).

[43]A. J. Newell, W. Williams, and D. J. Dunlop, J. Geophys. Res.: Solid Earth **98**, 9551, https://doi.org/10.1029/93JB00694 (1993).

[44]S. V. Komogortsev, R. S. Iskhakov, and V. A. Fel'k, J. Exp. Theor. Phys. **128**, 754 (2019).

[45]J. Walowski, M. D. Kaufmann, B. Lenk, C. Hamann, J. McCord, and M. Munzenberg, J. Phys. D: Appl. Phys. **41**, 164016 (2008).

[46]D. Kumar, O. Dmytriiev, S. Ponraj, and A. Barman, J. Phys. D: Appl. Phys. **45**, 015001 (2012).

[47]C. C. Dantas and L. A. de Andrade, Phys. Rev. B **78**, 024441 (2008).

[48]R. N. Yaroslavtsev, L. A. Chekanova, S. V. Komogortsev, and R. S. Iskhakov, Solid State Phenom. **215**, 237 (2014).

[49]H. Min Zhang, X. Li Zhang, J. Jing Zhang, Z. Yue Li, and H. Yuan Sun, J. Electrochem. Soc. **160**, D41 (2013).

[50]E. Denisova, L. Chekanova, R. Iskhakov, S. Komogortsev, I. Nemtsev, D. Velikanov, and S. Mel'nikova, Solid State Phenom. **233**, 583 (2015).

[51]A. Baker *et al.*, J. Magn. Magn. Mater. **421**, 428 (2017).

[52]K. Rivkin and J. B. Ketterson, J. Magn. Magn. Mater. **306**, 204 (2006).

[53]S. Jung, J. B. Ketterson, and V. Chandrasekhar, Phys. Rev. B **66**, 132405 (2002).

[54]R. D. McMichael and M. D. Stiles, J. Appl. Phys. **97**, 10J901 (2005).

[55]M. d'Aquino, C. Serpico, and C. F. G. Miano, J. Comput. Phys. **228**, 6130 (2009).

[56]V. A. Ignatchenko and V. A. Felk, Phys. Rev. B **71**, 094417 (2005).

[57]V. A. Ignatchenko and V. A. Felk, Phys. Rev. B **74**, 174415 (2006).

[58]V. A. Ignatchenko and V. A. Felk, Phys. Met. Metallogr. **100**(Suppl. 1), 63 (2005).

[59]W. Xu, D. B. Watkins, L. E. DeLong, K. Rivkin, J. B. Ketterson, and V. V. Metlushko, J. Appl. Phys. **95**, 6645 (2004).

[60]S. Jung, B. Watkins, L. DeLong, J. B. Ketterson, and V. Chandrasekhar, Phys. Rev. B **66**, 132401 (2002).

[61]S. V. Komogortsev, R. S. Iskhakov, P. A. Kuznetsov, A. I. Belyaev, G. N. Bondarenko, and L. A. Chekanova, Phys. Solid State **52**, 2287 (2010).

[62]R. S. Iskhakov, E. A. Denisova, S. V. Komogortsev, L. A. Chekanova, Y. E. Kalinin, and A. V. Sitnikov, Phys. Solid State **52**, 2263 (2010).

[63]D. Kumar and A. O. Adeyeye, J. Phys. D: Appl. Phys. **50**, 343001 (2017).

[64]N. Dao, M. J. Donahue, I. Dumitru, L. Spinu, S. L. Whittenburg, and J. C. Lodder, Nanotechnology **15**, S634 (2004).

[65]Y. P. Ivanov, M. Vázquez, and O. Chubykalo-Fesenko, J. Phys. D: Appl. Phys. **46**, 485001 (2013).

[66]J. Prat-Camps, C. Navau, D.-X. Chen, and A. Sanchez, IEEE Magn. Lett. **3**, 0500104 (2012).

[67]C. Kittel, Phys. Rev. **73**, 155 (1948).

[68]A. G. Gurevich and G. A. Melkov, *Magnetization Oscillations and Waves* (CRC Press, Boca Raton, FL, 1996).

[69]R. E. Arias, Phys. Rev. B **94**, 134408 (2016).

[70]T. K. Das and M. G. Cottam, J. Appl. Phys. **109**, 07D323 (2011).

[71]S. A. Nikitov, A. R. Safin, D. V. Kalyabin *et al.*, Phys. Usp. **63**, 10 (2020).

[72]G. N. Kakazei, A. F. Kravets, N. A. Lesnik, M. M. P. de Azevedo, Y. G. Pogorelov, and J. B. Sousa, J. Appl. Phys. **85**, 5654 (1999).

[73]A. Encinas-Oropesa, M. Demand, L. Piraux, I. Huynen, and U. Ebels, Phys. Rev. B **63**, 104415 (2001).

[74]V. Fel'k and S. Komogortsev (2021). "Data for ferromagnetic resonance simulation in a microtube," Materials Cloud 2021.44.